Macromolecules

ARTICLE

pubs.acs.org/Macromolecules

Crystallinity and Chain Conformation in PEO/Layered Silicate Nanocomposites

K. Chrissopoulou,*[,†] K. S. Andrikopoulos,[‡] S. Fotiadou,[†,§] S. Bollas,[†] C. Karageorgaki,[†,§] D. Christofilos,[‡] G. A. Voyiatzis,[∥] and S. H. Anastasiadis[†,⊥]

[†]Institute of Electronic Structure and Laser, Foundation for Research and Technology - Hellas, P.O. Box 1527, 711 10 Heraklion Crete, Greece

[‡]Physics Division, School of Technology, Aristotle University of Thessaloniki, 541 24 Thessaloniki, Greece

[§]Department of Chemical Engineering, Aristotle University of Thessaloniki, 541 24 Thessaloniki, Greece

[∥]Institute of Chemical Engineering & High Temperature Chemical Processes, Foundation for Research and Technology - Hellas, P.O. Box 1414, 265 04 Patras, Greece

[⊥]Department of Chemistry, University of Crete, P.O. Box 2208, 710 03 Heraklion Crete, Greece

ABSTRACT: The polymer chain conformation under confinement and the morphology of the nanohybrid materials are investigated in hydrophilic polymer/layered silicate nanocomposites. A series of poly(ethylene oxide)/sodium montmorillonite hybrids were synthesized utilizing melt intercalation with compositions covering the complete range from pure polymer to pure clay. Intercalated nanocomposites with mono- and bilayers of PEO chains are obtained in all cases. The intercalated chains as well as the ones adsorbed on the outer surface of the clay particles remain purely amorphous; their conformation, however, exhibits different characteristics from those of the amorphous neat polymer melt. It is only for compositions where a large amount of excess polymer exists outside the completely full galleries that the polymer crystallinity is recovered.

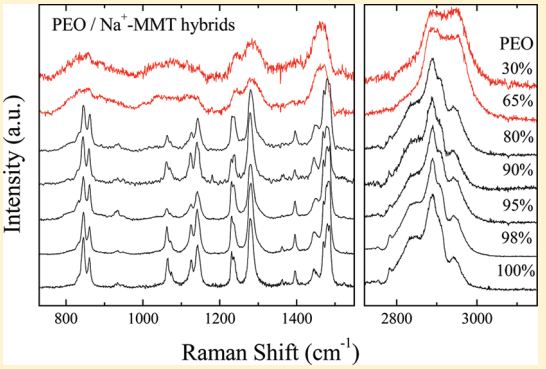

I. INTRODUCTION

Polymer materials are often filled with inorganic compounds in order to improve their properties. Over the past decade, attempts have been made to circumvent the compromises required in material design by utilizing nanoparticles as the inorganic additives, which, when dispersed within the polymeric matrix, produce a nanocomposite;[1] in these cases the final properties of the hybrids are determined mainly by the existence of many interfaces.[2] Of particular interest among different organic/inorganic nanohybrids are polymer/layered silicate nanocomposites, which constitute a relatively new class of materials that has attracted growing scientific and technological interest due to their unique properties, which make them candidates for a number of potential applications.[3−12]

Mixing polymers with layered inorganic materials can lead to three different types of structure, depending on the specific interactions between the two components:[3,5] the phase separated, where the two components are immiscible, the intercalated, in which the polymer chains reside within the inorganic galleries forming thin polymer films with 0.8−2.5 nm thickness, and the exfoliated one, where the interactions between the chains and the surfaces are very favorable that the layered structure of the inorganic material is destroyed, resulting in dispersed platelets within the polymer matrix. The best properties of the hybrids are usually observed for intercalated[13−16] or exfoliated systems.[17−21] Moreover, intercalated nanohybrids are model systems for the investigation of the static and dynamic properties of macromolecules in nanoconfinement, using, however, macroscopic samples and conventional analytic techniques.[22−31]

Natural layered silicates are mostly hydrophilic, and their interactions are favorable only with polar polymers.[13,27,30,32−34] In the case of hydrophobic polymers, intercalation or exfoliation can be achieved only with organophilized clays, i.e., with materials where the hydrated cations within the galleries are replaced by proper surfactants (e.g., alkylammonium) via a cation exchange reaction.[14,29,35] In the case of even less polar polymers, like polyolefins, the use of appropriate compatibilizers is necessary in order to control the interactions and achieve exfoliation.[17,19,36−39]

Despite the fact that the desired structure can be frequently achieved and the improvement of mechanical,[40] thermal,[41] flammability,[42] or barrier properties[43] has been reported in certain cases, the behavior has not been fully understood. Moreover, other factors like the preparation and processing methods appear to be involved in the complex structure−properties relation.[44,45]

Received: July 25, 2011
Revised: October 25, 2011
Published: November 18, 2011

Additionally, in the case of semicrystalline polymers, the influence of the addition and the state of dispersion of the nanofillers on the conformation of the chains and/or on crystallization has been largely overlooked.

Poly(ethylene oxide), PEO, is a nonionic, water-soluble, semicrystalline polymer with many applications due to its flocculent, thickening, sustained-release, lubrication, dispersing, and water-retention properties. Its hydrophilicity, biocompatibility, and versatility make it attractive as a biomaterial as well. Additionally, PEO is a favorable candidate for the development of solid polymer electrolytes with high ionic conductivity because of its ability to dissolve large amounts of salt and its structure, which supports ion transport.[13,22,46,47] Despite its pronounced crystalline character that inhibits the cation mobility, PEO-based electrolytes are still among the most studied polymer ionic conductors, whereas various methods have been developed to increase the volume fraction of its amorphous phase and to improve its conductivity at ambient temperatures.[46,48] A promising way to control polymer crystallinity is the incorporation of inorganic nanoparticles such as nanoclays;[13,49,50] this can additionally increase the mechanical and thermal stability of the material and, thus, improve its final performance.

In spite of the increasing interest in PEO/layered silicate nanocomposites, the findings concerning the effects of the inorganic filler on crystallization and polymer chain conformation are still controversial. The inorganic surface has been shown to favor a nucleating effect for various polymers,[51] whereas reduction of heterogeneous nucleation has been reported for PEO due to PEO/Na^+ coordination.[52] Moreover, there have been contradictory reports on the conformation of the chains, which reside between or adjacent to the inorganic layers for intercalated PEO nanocomposites. In one case, the preservation of the PEO helical structure inside the galleries with the cations located in the center of the helix was proposed[53] with hydrogen bonds being formed between the water molecules of the coordination shell of the intergallery cations and ethylene oxide monomers, which result in incomplete water replacement by the polymer. In another case, however, a highly distorted helical structure was proposed to be a better description of the conformation of PEO chains inside the galleries of layered silicates.[44] Alternatively, it was suggested that the PEO chains within the galleries are not helical but they resemble single or double adsorbed polymer layers onto the clay surfaces.[54] Computer simulations have been used to explore the chain configuration within the confining space; they suggested that PEO intercalates between the layers by replacing partly or completely the weakly adsorbed water molecules. Polymer chains are arranged in discrete layers parallel to the crystalline silicate layers retaining a disordered, liquidlike structure with no crystallinity and no preferential ordering of the C−C−O bonds.[55] Actually, it was suggested that, for all temperatures simulated, the PEO chains within the galleries are less ordered than the most disordered bulk PEO systems;[56,57] that was attributed to both the strong spatial confinement and to the strong coordination of the ether oxygens with the alkali cations present in the galleries.

In this paper, we systematically study the effect of incorporation of inorganic material and elucidate the influence of the severe confinement on the structure and conformation of polymer chains in PEO/Na^+-MMT nanohybrids. A series of composites with PEO content that covers the whole regime from pure polymer to pure clay were utilized and characterized by X-ray diffraction and differential scanning calorimetry. In all cases, intercalated nanocomposites with mono- and bilayers of PEO chains were obtained. We show that for low polymer concentrations, where all the polymer chains are intercalated, PEO is purely amorphous, and it is only when there is excess polymer outside the completely full galleries that the bulk polymer crystallinity is recovered. Moreover, vibrational spectroscopy (Raman and FTIR) has been utilized to quantitatively probe the conformation of the amorphous polymer chains in the nanohybrids relative to that of neat PEO melt.

II. EXPERIMENTAL PART

Materials. Poly(ethylene oxide) homopolymer, PEO, was purchased from Aldrich. Its molecular weight is 100 000 g/mol and its polydispersity index is M_w/M_n = 2.4, as determined by size exclusion chromatography utilizing polystyrene standards. The polymer possesses hydroxyl chain ends. It exhibits a glass transition temperature $T_g = -67$ °C and a melting temperature T_m = 65 °C. The layered silicate is a hydrophilic sodium-activated montmorillonite, Na^+-MMT (Southern Clay). It has a cation exchange capacity (CEC) of 92.6 mmol/100 g, and it was used following heating at 120 °C overnight in a vacuum oven to allow removal of excess water molecules from the hydrophilic galleries. The presence of hydrated Na^+ makes the galleries hydrophilic so that polar polymers like PEO can mix without the need of modification of the silicate hosts. PEO/Na^+-MMT nanocomposites were synthesized by direct melt intercalation; the two components were mixed in the appropriate amounts, ground in a mortar to get a fine powder, and annealed in a vacuum oven at 100 °C for 2 days. Following the melt intercalation, the temperature for all specimens decreased from 100 °C to room temperature very slowly to ensure equilibrium and the highest degree of crystallinity (for each composition). Moreover, all measurements were performed a few days after the sample preparation, ensuring that the kinetics of crystallization would not interfere at all with the present investigation. The compositions studied cover the complete range from pure polymer to pure clay.

Experimental Techniques. *X-ray Diffraction (XRD).* Structural characterization of the pure materials and of the nanocomposites was performed with X-ray diffraction, using a RINT-2000 Rigaku diffractometer. The X-rays are produced by a 12 kW rotating anode generator with a Cu anode equipped with a secondary pyrolytic graphite monochromator. The Cu Kα radiation was used with wavelength $\lambda = \lambda_{CuK\alpha}$ = 1.54 Å. Measurements were performed for 2θ from 1.5° to 30° with step of 0.02°. A Rigaku multipurpose high temperature attachment was utilized so that measurements at ambient temperature and at 90 °C (above the melting temperature of the polymer) could be performed at the same setup without changing the sample geometry; these measurements were utilized for the crystallinity calculation. In all cases, samples that were crystallized from the melt with a cooling rate of 10 °C/min were first measured at ambient temperature, whereas the measurement in the melt followed. Materials with periodic structure like the layered silicate clays show characteristic (00l) diffraction peaks, which are related to the spacing of the layers according to Bragg law, $n\lambda = 2d_{00l} \sin\theta$, where λ is the wavelength of the radiation, d_{00l} is the interlayer distance, 2θ is the diffraction angle, and n the order of the reflection.

Differential Scanning Calorimetry (DSC). The thermal properties of the nanocomposites as well as of the initial components were measured with a PL-DSC (Polymer Laboratories) differential scanning calorimeter. The temperature range covered was between −100 and 120 °C with a heating/cooling rate of 10 °C/min, whereas two heating/cooling cycles were performed in all cases. The melting, T_m, and crystallization, T_c, temperatures were obtained from the second cycle to ensure the elimination of the effects of thermal history. All the measurements were performed under nitrogen flow to prevent the decomposition of the samples. Controlled cooling was achieved using liquid nitrogen.

Thermogravimetric Analysis (TGA). The nanocomposites were characterized with thermogravimetric analysis (TGA) on a SDT600 TGA/DTA apparatus (TA Instruments). Heating scans were performed from room temperature to 500 °C at a heating rate of 10 °C/min under an argon atmosphere. TGA measurements were important to verify the composition of the final specimens versus the designed composition. The remaining weight at temperatures above 500 °C, where PEO had decomposed, was 10.4% for the 90 wt % PEO hybrid, 19.3% for the 80 wt % PEO hybrid, 34.4% for the 70 wt % PEO hybrid, 47.7% for the 60 wt % PEO hybrid, 54.1% for the 50 wt % PEO hybrid, and 59.8% for the 40 wt % PEO hybrid.

Raman Spectroscopy (RS). Poly(ethylene oxide) crystallinity as well as the conformations of PEO chains in the amorphous state were investigated by Raman Spectroscopy (RS) utilizing two different experimental setup. (a) Initially, a THR-1000 single spectrograph equipped with a liquid nitrogen cooled CCD detector was used. The beam of a HeNe laser (λ_{exc} = 632.8 nm) was properly focused on the sample by a 50× objective, and the collected light in the backscattering geometry was directed to an appropriately positioned Notch filter and then transferred through an optical fiber and focused on the entrance slit of the monochromator (no polarization preferences were selected for the scattered radiation). The resolution was better than 2 cm^{-1} over the whole spectral range. (b) For the high temperature measurements of bulk PEO, a homemade optical furnace was utilized supported by a temperature controller (temperature stabilization better than ±1 °C). The optical furnace was suitably placed in the compartment of a FRA-106/S Raman component of an Equinox 55 Bruker spectrometer so that backscattered spectra can be recorded (spectral resolution set at 2 cm^{-1}). FT-Raman spectra were obtained with NIR excitation at 1064 nm (via an R510 diode pumped Nd:YAG laser). In order to avoid polymer degradation, the neat PEO sample was placed in a thoroughly cleaned Pyrex tube and was subsequently sealed under vacuum (~10^{-5} bar). Because of the fact that strong fluorescence background of the neat inorganic component (Na^+-MMT) prohibited the inspection of the Raman bands when excitation wavelengths at 1064 or 632.8 nm were used, the utilization of a micro-Vis/UV Raman spectrometer (Labram HR-800 spectrograph of JY/Horiba) with an excitation line at 441.6 nm of an air-cooled HeCd laser (dual, 325/442 nm, UV/blue, 20/80 mW; IK5651R-G model laser of Kimmon Electric Co.) was essential for the recording of its RS with a spectral resolution of ~3 cm^{-1}.

Attenuated Total Reflectance–Fourier Transform Infrared Spectroscopy (ATR-FTIR). The conformations of the PEO chains in the bulk and in the hybrid materials were further investigated at ambient conditions as well as at high temperatures by ATR-FTIR. The IR spectra of the different samples were recorded by an Equinox 55 Bruker spectrometer using a DTGS detector (spectral resolution was set at 3 cm^{-1}). For the high temperature measurements a single reflection diamond ATR accessory of Golden Gate was properly attached to the FTIR instrument. Temperature was controlled with accuracy better than ±1 °C. In order to maintain an inert atmosphere during the high temperature experiments, the sample compartment was properly flushed with nitrogen for 30 min before each measurement. For background correction purposes, corresponding spectra were recorded for each temperature. Special care was given so that no bands associated with CO_2 or H_2O were present after the background correction.

III. RESULTS AND DISCUSSION

X-ray Diffraction. Figure 1 shows the X-ray diffraction patterns of PEO, Na^+-MMT, and of PEO/Na^+-MMT nanocomposites with varying polymer concentration. Pure Na^+-MMT exhibits a main (001) diffraction peak at 2θ = 8.8°, which corresponds to an interlayer distance of 1.0 nm. Upon addition of only 5 wt % PEO, this peak disappears and two other peaks emerge at 2θ = 6.7° and 2θ = 4.8°, corresponding to interlayer distances of 1.30 and 1.85 nm, respectively. The appearance of those peaks indicates

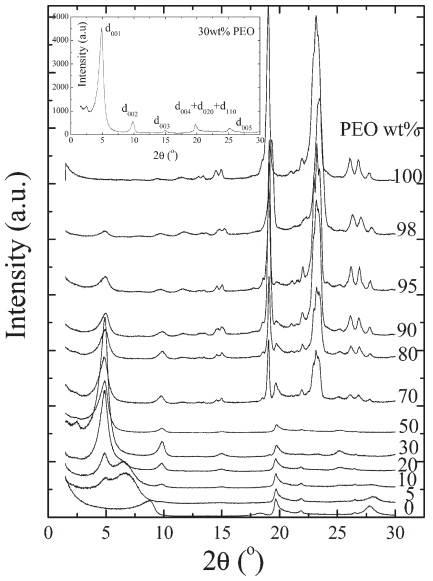

Figure 1. X-ray diffractograms of pure PEO (top), Na^+-MMT (bottom), and PEO/Na^+-MMT nanocomposites with varying polymer content. The curves have been shifted vertically for clarity. The inset illustrates the X-ray diffractogram of the 30 wt % PEO/Na^+-MMT nanocomposite where the higher order 00*l* reflections have been identified.

that PEO chains have intercalated between the inorganic layers, forming mono- and bilayers of polymer chains within the interlayer galleries. As PEO concentration increases up to 20 wt %, the relative intensities of the two peaks change; the one corresponding to d = 1.85 nm increases, indicating the formation of more bilayer filled galleries, while the intensity of the first peak decreases. By further increasing the PEO concentration to 30 and 50 wt %, only bilayers of intercalated PEO chains are observed as evidenced by the XRD peak at 2θ = 4.8°, which is the only one observed in the low 2θ range.[27] The inset of Figure 1 shows the X-ray diffractograms of PEO/Na^+-MMT nanocomposites containing 30 wt % PEO where the existence of five orders of 00*l* reflections of the intercalated structure can be identified (although the 004 one appears together with those of different crystallographic planes of montmorillonite (020 and 110)); this demonstrates clearly the coherence of the intercalated structure. Equally important, in this composition range, is the fact that no peaks are observed at higher angles that could be assigned to the crystalline structure of PEO. Thus, for polymer concentrations up to 50 wt %, single and double layers of intercalated polymer coexist inside the inorganic galleries with no evidence of crystalline phase, in agreement with simulation results that predict a disordered liquidlike structure inside the galleries.[55,56] It is noted that a similar series of nanocomposites that were prepared utilizing solution intercalation gave exactly the same results, thus certifying the attainment of equilibrium in both cases.

Poly(ethylene oxide) is a semicrystalline polymer that crystallizes in a monoclinic unit cell. Its crystalline structure has been studied in the past with a series of experimental techniques like X-ray diffraction and infrared and Raman spectroscopies. The majority of the studies has resulted in that the most plausible model to describe its structure is the 7_2 helical model, which assumes seven chemical units and two turns within the helix period (which coincides with the *c*-axis) of 19.4 Å.[58] At the same time, a planar zigzag crystal structure of PEO was reported for a stretched specimen about 2-fold after necking at ambient

Table 1. Crystallographic Data for Crystalline PEO

	helical structure		transplanar structure	
$2\theta_{obs}$ (deg)	2θ (deg)[60,61]	*hkl*	2θ (deg)[59]	*hkl*
13.4	13.42	100		
14.5	14.53	021		
14.9	15.2, 14.9	110		
	17.1	101		
19.0	18.9, 19.2	120		
21.0	20.80	031	20.44	100
21.4	21.1	104		
21.9	21.88	102		
	22	023		
	22.8, 23.26	112		
23.2	23.2	032		
24.0	24.1	130	24.36	010
			25.13	110
26.1	26.2	033		
26.8	26.7	131		
27.8	27.5	200	27.41, 28.39	012, 002
			30.79	112
	32.0	211	32.89	102

temperature.[59] The scattering angles of the main X-ray diffraction peaks of PEO homopolymer (Figure 1) are in a very good agreement with those reported in the literature for the helical model of the crystalline PEO and are shown in Table 1 along with their *hkl* indexing.[59−61]

The diffractograms of the nanocomposites show peaks that correspond to those of crystalline PEO only for polymer concentrations 70 wt % and higher. Their absence from the XRD patterns of the nanocomposites with lower PEO content indicates that the intercalated polymer as well as the chains that are in close proximity to the inorganic surfaces are amorphous; it is only the excess polymer outside the completely filled galleries and away from the outside walls of the inorganic particles (in the hybrids with high concentration) that is able to crystallize. The positions of the crystalline peaks, when present, are very similar to those of pure PEO; nevertheless, on a closer examination two small peaks at $2\theta = 24.4°$ and $2\theta = 25.2°$ are observed in the presence of the inorganic material, the position of which is very close to the ones reported for the transplanar PEO crystalline structure.

In an attempt to quantify our results, the X-ray diffractograms over a specific angular range of 10°−30° were fitted with a linear combination of a certain number of Pearson functions one for each of the main crystalline peaks and of a Lorentz function[62] that accounts for the amorphous part and is obtained from fitting the corresponding measurement of the melt at 90 °C. Figure 2 shows the diffractograms together with the fitted curve for the pure PEO and a nanocomposite containing 10 wt % clay and 90 wt % polymer. Note that the measurements at ambient temperature and those at 90 °C (above the melting temperature) were performed with the identical sample utilizing the temperature cell. It is clear that the fitted curve follows the experimental data very well. Similar fittings have been obtained for all nanocomposites with high polymer content. The crystallinity values can be obtained from the integrated intensity of all crystalline reflections

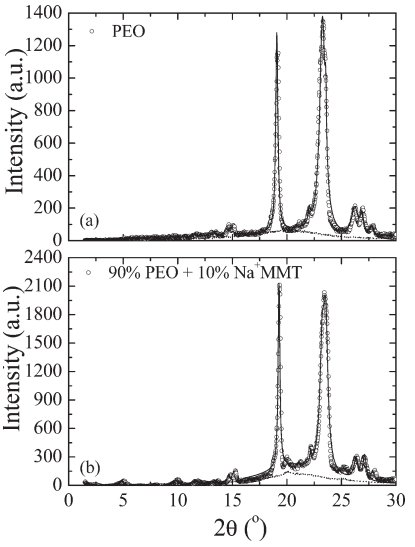

Figure 2. Fitting of the X-ray diffractograms of (a) pure PEO and (b) a PEO/Na^+-MMT nanocomposite containing 90 wt % PEO and 10 wt % Na^+-MMT. The solid lines correspond to the total fit (see text). The diffraction data of the same specimens measured at 90 °C in the melt state are shown with the dotted lines.

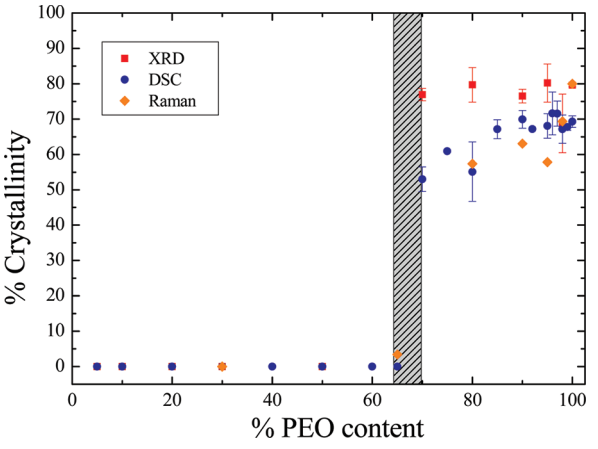

Figure 3. Degree of crystallinity as a function of PEO content obtained from the analysis of X-ray diffraction (filled squares), differential scanning calorimetry (filled circles), and Raman spectroscopy (filled diamonds) measurements.

(I_c) and of the amorphous halo (I_a) as $X_c = [I_c/(I_c + I_a)]$; these values are shown in Figure 3.[63]

It is obvious that the polymer crystallinity in the nanocomposites with more than 70 wt % polymer is rather constant and practically independent of the polymer content. It is striking that in hybrids with polymer content less than 70 wt % there are no crystalline peaks; thus, the crystallinity (at least according to the resolution of X-ray diffraction) drops abruptly to zero. Nevertheless, it is noted that, although the presence of the jump in the values of crystallinity is beyond any doubt, the exact composition where this jump occurs may weakly depend on the sample preparation and its thermal history as well as polymer molecular characteristics;[64−67] however, this was not investigated any further in the present work. The composition range that may be affected is shown highlighted in Figure 3. The percentage of

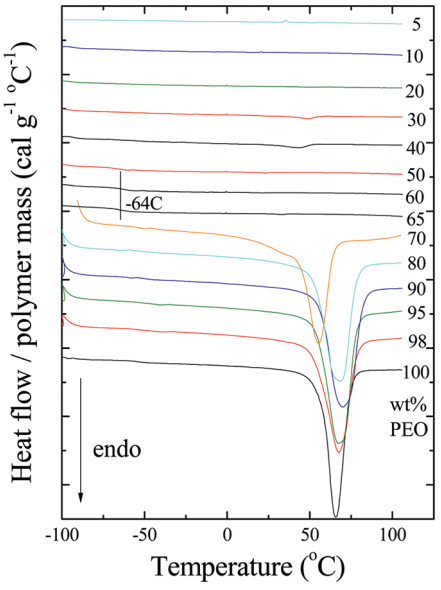

Figure 4. Differential scanning calorimetry thermograms of PEO, Na^+-MMT, and PEO/Na^+-MMT nanocomposites with varying polymer content; the data are shown for the second heating. The curves have been shifted vertically for clarity. Heating rate: 10 °C/min.

crystallinity in these nanohybrid materials derives from two controversial effects: the enhancement of crystallization in the presence of inorganic fillers and, at the same time, its hindrance due to the addition of alkali cations and their coordination with the polymer chains as well as the confinement of the polymer chains.[52,56] In agreement with earlier simulation results,[56] the intercalated PEO chains are indeed in an amorphous, liquidlike state. Nevertheless, a simple calculation based on the measured interlayer distances of the pure and intercalated Na^+-MMT as well as the densities of PEO (1.13 g/cm^3 at 25 °C, Aldrich) and clay (2.86 g/cm^3, Southern Clay) results in that the necessary polymer to completely fill the galleries is about 21 wt %, i.e., a 79:21 clay-to-polymer ratio. This calculation in conjunction with our analysis results indicates that it is not only the intercalated polymer that is amorphous but a large fraction of the polymer that is in excess outside the galleries. Most probably, this is related to polymer chains adsorbed onto the outer surfaces of the clay particles due to the favorite PEO/clay interactions. The maximum PEO content for which no crystallinity is observed should depend on the outer organic−inorganic interface. The width of the main diffraction peaks of the nanocomposite can be used to extract information on the particle size through the Scherrer equation;[68] this analysis results in that there are only 4−5 inorganic layers per particle. Thus, a polymer layer of ∼5−10 nm is estimated to be adsorbed on the outer inorganic surface for hybrids where crystallization is hindered in agreement with earlier studies on silica nanocomposites.[69]

Differential Scanning Calorimetry. These results are further verified by DSC measurements that are shown in Figure 4; a melting endotherm is observed only for high polymer concentrations. In all cases the measured heat flow is shown normalized with the polymer mass of the nanocomposite and the heating rate so that the integral under the melting curve will directly provide the heat of fusion, ΔH_{exp}. It is noted that, in the nanocomposites, it is only the polymer that undergoes the melting transition; thus, the contribution of the inorganic material to the C_p is a constant factor that does not influence the enthalpy calculation. It is obvious that only nanocomposites with polymer content 70 wt % or higher exhibit a melting transition (and the respective crystallization), whereas hybrids with lower polymer content are completely amorphous in perfect agreement with the XRD results.[70,71] The degree of crystallinity of the hybrids can be calculated as % crystallinity = $\Delta H_{exp}/\Delta H_{cryst}$, where ΔH_{exp} the measured heat of fusion of the polymer in the nanocomposite and ΔH_{crys} = 196.4 J/g the heat of fusion of a totally crystalline poly(ethylene oxide). The values of the degree of crystallinity obtained from DSC are plotted in Figure 3 together with the respective results obtained by XRD. In general, the values of crystallinity obtained by the two techniques are in close agreement with the ones derived from DSC showing a small decrease with decreasing polymer content. Nevertheless, the important finding of the discontinuity in the crystallinity and its abrupt drop to zero is evident by both techniques. Relatively good agreement[72] or parallel behavior[73,74] between results of XRD and DSC concerning polymer crystallization have been reported earlier as well, whereas, when differences were observed, they were attributed to the inherent heating involved in calorimetry, which induced crystallization of the tested samples.[75]

Furthermore, in most of our nanocomposites the glass transition seems to be completely suppressed; the hybrids with very low polymer content showed no evidence of T_g, in agreement with previous studies either because of the low polymer content or due to the suppression of the glass transition because of the strong confinement.[27,32] On the other hand, the hybrids with more than 70−80 wt % polymer exhibit a high degree of crystallinity, and thus, the amorphous part that exhibits a glass transition is very small. Therefore, it is only for compositions of 50−65 wt % PEO that a weak glass transition appears at T = −64 °C, which is in a good agreement with the expected glass transition temperature of bulk PEO, indicating that the behavior of amorphous PEO chains away from the silicate surfaces is very similar to those in the bulk.

Vibrational Spectroscopy. Experimental techniques like XRD and especially DSC are widely utilized to provide a quantitative measure of the polymer crystallinity. However, its determination is based on the assumption of a two-phase structure; more detailed investigations utilizing vibrational spectroscopy show that a simple two-phase model is only an approximation.[76] Vibrational spectroscopy, like Raman and infrared, has been utilized to probe the conformational state of polymer chains. Despite the difficulties to quantitatively estimate polymer crystallinity utilizing Raman spectroscopy, good agreement has been recently obtained with DSC experiments for isotactic poly(propylene).[77] In the following, Raman and IR are utilized to probe the polymer crystallinity in the nanohybrids and to investigate the chain conformation of the liquidlike polymer confined within the inorganic galleries relatively to that of the polymer melt.

The repeat unit of poly(ethylene oxide) consists of three linkages along the backbone: the O−C, C−C, and C−O bonds. Steric consideration alone would suggest that the minimum-energy conformation is the all-trans, *ttt*. However, the most stable conformation in the crystal includes a gauche conformation, which is designated *tgt* (which means that the majority of the C−C bonds are in the gauche and the majority of the O−C and the C−O bonds in the trans conformation) derived from electrostatic interactions between net positive and negative charges that accumulate on the backbone.[58,78,79]

Figure 5 shows the Raman spectra of PEO and of nanocomposites with different polymer concentrations. It is clear that the

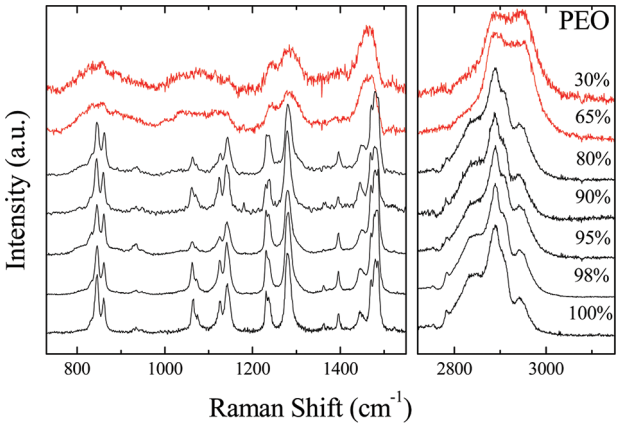

Figure 5. Raman spectra of PEO and of PEO/Na^+-MMT nanocomposites with different polymer concentrations at ambient temperature.

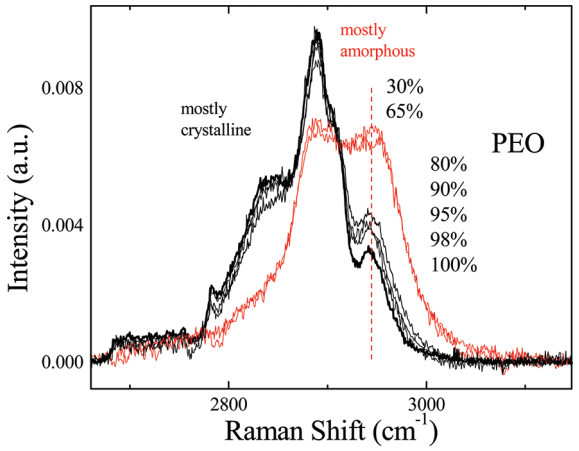

Figure 6. Normalized Raman spectra of PEO and PEO/Na^+-MMT nanohybrids with different polymer concentrations at ambient temperature. The spectra are normalized so that the total integrated intensity of the bands appearing within this spectral region is constant for all compositions (see text). The dashed line indicates the frequency where there is a strong contribution of the amorphous phase.

spectra of neat PEO as well as of the hybrids with high polymer content are dominated by sharp vibrational bands due to the crystalline phase of the polymer. On the other hand, the Raman spectra of the hybrids with 65 and 30 wt % PEO are significantly different, showing peak shifts and/or mainly very broad features. The bands appearing in these spectra are comparable to the Raman bands of PEO melt, as will be further discussed below, apart from the relative intensities of certain bands; in these cases the polymer is mainly amorphous.[80] This finding is consistent with both the XRD and the DSC data that show Bragg reflections and melting endotherms only for high concentration of PEO whereas the hybrids with less than 70 wt % PEO appear amorphous-like; Raman scattering verifies that the polymer chains for concentrations below 70 wt % are indeed amorphous. Moreover, inspection of the Raman measurements of the hybrids with high polymer concentration indicates that the contribution of the amorphous phase to the total Raman spectrum (amorphous and crystalline) becomes more important as the concentration of the polymer decreases.

One of the common methodologies introduced in order to estimate the crystallinity of polymers by Raman spectroscopy is to identify two well-defined bands in the Raman spectrum, which can be attributed to a certain vibration in the crystalline and the amorphous phases, respectively, and to calculate the ratio of the corresponding integrated intensities. However, vibrational modes that belong totally to amorphous and/or to crystalline phases cannot be separately allocated in the spectrum of PEO. Therefore, the calculation of PEO crystallinity was performed utilizing the spectral region assigned to C−H stretching vibrations with the extra assumption that the Raman cross section of the vibrational modes belonging to species incorporated in the crystalline and amorphous regions of the structure are basically similar. In this case, the Raman intensities for a certain hybrid, with polymer concentration w %, will be given by

$$I_w = Aw(X_c I_{crystal} + (1 - X_c) I_{amorphous}) \quad (1)$$

where X_c is the crystallinity, $I_{crystal}$ is the intensity of the completely crystalline PEO, $I_{amorphous}$ is that of the completely amorphous one, and A is an experimental proportionality constant.

Figure 6 shows the Raman spectra of the hybrids in the frequency range of the most prominent contribution of the amorphous phase to the spectrum, i.e., in the spectral range of C−H stretching modes. The spectra are shown normalized so that the integrated intensity of all the bands appearing within this spectral region (2750−3050 cm^{-1}) is constant for all compositions. This normalization essentially takes care of the (Aw) term on the right side of eq 1, so they can be denoted as $I'_w = I_w/(Aw)$. The crystalline phase contributes mainly at 2840 and 2890 cm^{-1} while the amorphous phase possesses a strong peak at 2945 cm^{-1} (dashed line). The Raman spectrum obtained from the 30 wt % PEO hybrid was assumed to be the one corresponding to the totally amorphous PEO, and thus, $I_{amorphous}(k) = I'_{30}(k)$ since the Raman spectrum corresponds rather well to the respective one obtained from PEO melt (to be discussed below) and because XRD and DSC measurements indicate no crystallinity for this concentration. Moreover, the Raman spectrum of the neat PEO, denoted as $I'_{PEO}(k)$, was assigned to a crystallinity value X_0 based on the XRD and DSC data of Figure 3 ($X_0 \approx 0.8$ obtained from XRD). With these considerations, the PEO crystallinity in the hybrid can be obtained from the Raman data using the equation

$$I'_w = \frac{X_c}{X_0} I'_{PEO} + \left(1 - \frac{X_c}{X_0}\right) I'_{30} \quad (2)$$

It has to be pointed out that the Raman spectrum of the inorganic filler is generally very weak and furthermore possesses no vibrational modes in the spectral region selected for the calculation of the crystallinity.

The spectra of Figure 6 were analyzed utilizing eq 2, and the obtained crystallinities are also plotted as a function of PEO concentration in Figure 3. The crystallinity values and their dependence on concentration are in good agreement with those obtained by XRD and DSC with small differences in their absolute values. Moreover, the striking feature is that all the techniques employed indicate that there exists a steplike dependence of the crystallinity on the weight fraction of PEO. It is worth noting that, whereas at ∼20−30 wt % PEO the galleries are totally filled with polymeric bilayers, the crystallinity is zero up to a remarkably higher amount, ∼65−70 wt %. This observation suggests that the inorganic particles of the hybrid

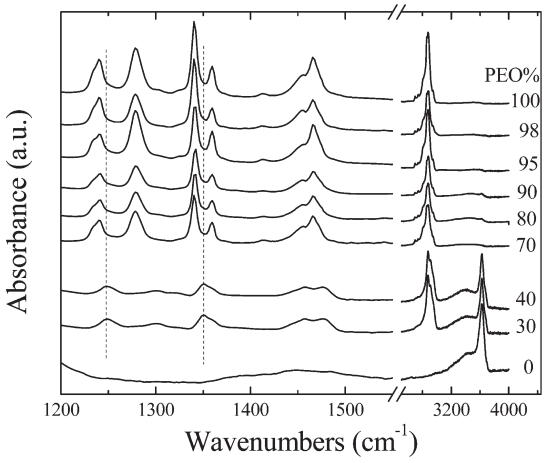

Figure 7. ATR-FTIR spectra of pure PEO, Na^+-MMT, and PEO/Na^+-MMT nanocomposites measured at ambient temperature with different polymer content as indicated.

material hinder the crystallization of not only the intercalated polymer chains but also those that comprise the organic–inorganic interface.

Complementary information with that obtained with Raman spectroscopy can be obtained utilizing FTIR spectroscopy. It is noted that the use of FTIR-ATR was chosen instead of the more traditional FTIR, which is widely used in similar studies, to avoid the use of KBr, the presence and the hydrophilicity of which might seriously disturb the PEO crystalline structure and affect the evaluation of chain conformation. Figure 7 shows the infrared spectra, measured at ambient temperature, of the pure polymer, the Na^+-MMT and the nanohybrids with varying amount of polymer. Pure PEO shows a large broad band of asymmetric $-CH_2$ stretching between 3000 and 2750 cm^{-1}. Moreover, the bands at 948 and 964 cm^{-1} (this spectral region is not shown since the clay exhibits a very broad peak covering the range 750–1200 cm^{-1} that dominate in the spectra of the hybrids) are assigned to the symmetric and asymmetric CH_2 rocking modes, the bands at 1236 and 1242 cm^{-1} are ascribed to the asymmetric CH_2 twisting modes, and the bands at 1343 and 1360 cm^{-1} are attributed to the asymmetric and symmetric CH_2 wagging modes, respectively. It has been well-known that the frequency, width, and intensity of these CH_2 vibrations are sensitive to the intermolecular interactions and the conformation changes of the polymer backbone. The spectra of all hybrids contain absorption bands characteristic of PEO superimposed with those of the layered silicate. Moreover, similarly with the Raman measurements, hybrids with polymer content higher than 70 wt % show sharp absorption bands that resemble the ones of pure PEO. On the contrary, hybrids with 30 and 50 wt % PEO, where the polymer is amorphous, show very broad peaks, shifted in a way that match the spectra and band assignment of PEO in the melt; for these hybrids instead of the asymmetric CH_2 twisting modes at 1242 and 1236 cm^{-1}, one band is observed at 1248 cm^{-1} and, instead of the asymmetric CH_2 wagging modes at 1360 and 1343 cm^{-1}, one band is observed at 1350 cm^{-1}.

It has, thus, been verified that the PEO chains within the inorganic galleries as well as a significant number of PEO chains that reside in close proximity to the outer surfaces of the inorganic particles remain in the amorphous state and cannot form a crystal. It is, therefore, understood that the inorganic

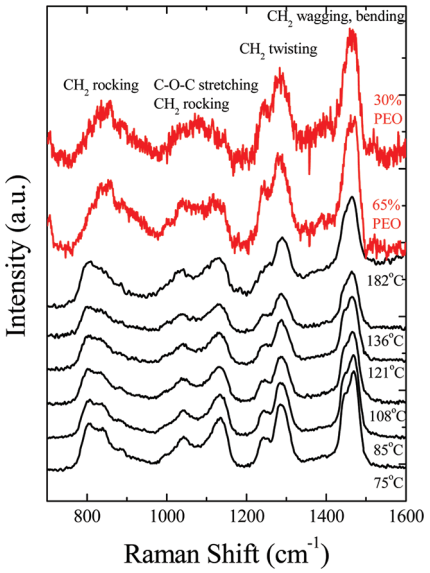

Figure 8. Raman spectra of pure PEO at 75, 85, 108, 121, 156, and 182 °C as well as of the 65 and 30 wt % PEO/Na^+-MMT nanocomposites (from bottom to top).

component constrains the chain segments on its surfaces and prevents them from acquiring the appropriate conformations that are required for the formation of the PEO crystal structures (e.g., the *tgt* conformation for the helical structure).

The conformational state of these confined or adsorbed chains can be investigated by Raman and IR spectroscopies using hybrids that do not show any crystal formation. Thus, the similarities and/or differences between their conformation and those of the chains in the respective amorphous bulk can be probed. The chain conformations in the amorphous glass are, ideally, those of the polymeric chains in the melt state at the vitrification temperature. Alternatively, instead of trapping the chain conformations in the glass, one can choose to perform *in situ* measurements on PEO melts at several temperatures.

Figure 8 shows the Raman spectra of PEO at different temperatures above T_m together with the spectra of two hybrids with 30 and 65 wt % PEO at ambient conditions in the spectral region where the CH_2 bending, wagging, twisting, and rocking modes as well as the C–O–C stretching mode appear. The spectra of the hybrids are indicative of totally amorphous polymeric materials since the main spectral features of PEO melt[81–83] can be easily recognized. The assignment of the different bands for the amorphous PEO can be found in Table 2. More specifically, the spectra can be tentatively divided into four spectral regions: the low wavenumber one (750–970 cm^{-1}) assigned to CH_2 rocking vibrations, the COC stretching vibrations at ~970–1200 cm^{-1}, the CH_2 twisting vibrations covering the region 1200–1350 cm^{-1}, and the CH_2 bending vibrations above 1400 cm^{-1}. Each of those four spectral regions contains envelopes of vibrational bands that are assigned to various chain conformational triads, i.e., *ttt*, *tgt*, *tgg*, and *ggg* (*t* and *g* stand for the trans and gauche conformation of triads of O–C, C–C, and C–O bonds, respectively). As can be clearly observed, differences in the polymer conformation can be monitored in the CH_2 rocking and COC stretching vibrations. Despite the fact that peak positions are essentially the same, the relative intensities of the peaks in each envelope seem to vary when temperature

Table 2. Assignment of the IR and Raman Bands for PEO in the Melt

peak position[a] Raman (cm^{-1})		peak position[a] FTIR (cm^{-1})			conformations PEO melt		
PEO melt (75 °C)	hybrid, 30% in PEO (ambient)	PEO melt (80 °C)	hybrid, 30% in PEO (ambient)	assignt	ref 81	ref 82	ref 83b
807	807	806	*b*	CH_2 rock	TGG	TTT	trans C−C
844	847			CH_2 rock	TTT, TTG, GTG	TGT	mostly gauche C−C, trans C−C
		850	*b*		TGG,GGG		mostly gauche C−C, trans C−C
885	890	880	*b*	CH_2 rock	GGG	TGG, GGG	trans C−C
927	932	920	*b*	CH_2 rock, C−O, C−C	TGG, GGG		gauche C−O
		944	*b*		TGT		gauche C−C
997	1006	994	*b*	C−O stretch, C−C stretch	TTT, TTG		trans C−C, gauche C−O
1041	1048	1036	*b*	CH_2 rock, COC stretch	TGG, TTT	TGG	trans C−C, gauche C−O
1100	1090	1094	*b*	C−O, C−C. CH_2 rock	all		
1136	1133	1135	*b*	COC stretch	all	TTT, TGT	
1242	1244	1248	1249	CH_2 twist	TGG, GGG	TGT, GGG	gauche C−C, trans C−O
1278	1277	1282	1284	CH_2 twist	TTT, TTG, GTG	TTT,TGT	all, trans C−O[83c]
1295	1295	1296	1300	CH_2 twist	all		gauche C−O
		1323	1322	CH_2 wag	TTT, TTG, GTG		trans C−C[83c]
		1350	1350	CH_2 wag	TGG, GGG		gauche C−C[83c]
1390				CH_2 wag			
	1428			CH_2 scissor			
1441	1452	1440	1446	CH_2 scissor	TGG, GGG	TGG, TGT	
		1457	1458	CH_2 scissor	TGT, TGG, GGG		
1468	1474	1471	1476	CH_2 scissor	TGT, TGG, GGG	TGT	all
		1485		CH_2 scissor	TTT, TTG, GTG		TGT

[a] Current work. [b] Spectral region severely screened by the strong inorganic bands.

increases in the amorphous melt as well as when the polymer chains are confined within the montmorillonite layers. More specifically, the intensity of the bands assigned to *ttt* conformations for most of the vibrations, i.e., for CH_2 rocking, COC stretching, and CH_2 twisting, appear modified if compared to the bands assigned to *tgg* or *ggg* conformations.

To investigate the changes in the conformations more quantitatively, the CH_2 rocking vibration region (750−970 cm^{-1}) was analyzed (Figure 9a) and the ratio I^{gauche}/I^{total} was calculated, where I^{gauche} is the intensity of the 835, 885, and 919 cm^{-1} band and I^{total} is the sum of the intensities of the 805, 835, 885, and 919 cm^{-1} bands. Figure 9a shows the spectra of the melt PEO at 75 °C and that of the hybrid with 30 wt % PEO at ambient temperature together with the total fit and the individual curves of four Gaussian bands for the different conformations of the CH_2 rocking vibrations. The results of the ratio I^{gauche}/I^{total} are shown in Figure 9b. This ratio for the neat polymer has a value close to 0.57 for the whole temperature range studied, and it does not show any significant temperature dependence. This indicates that there is a small preference for the gauche vibration of the C−C bond. In the case of the hybrid, however, this ratio possesses a much higher value even at ambient conditions (I^{gauche}/I^{total} = 0.72), which shows that the population of the C−C bonds with gauche conformation increases under confinement.[84] These results can be considered as direct experimental evidence of the existence of an amorphous phase both within the galleries of the nanocomposite and in close proximity to the outside walls of the inorganic particle, which is, however, significantly different than the melt of bulk PEO. It is noted, once more, that for the nanohybrid with 30 wt % PEO the majority of the polymer chains are intercalated and there is not much polymer in excess outside the completely filled galleries.

Figure 10 shows the ATR spectra of pure PEO melt (Figure 10a) and of a hybrid containing 30 wt % PEO (Figure 10b) measured at temperatures above the T_m of the polymer, in the spectral region where CH_2 bending, wagging, and twisting modes appear. The intensities of the characteristic PEO bands strongly depend on the conformational characteristics of the polymer chains as indicated by a number of works on PEO melts and solutions.[81,83] The assignment of the bands for the case of PEO melt is shown in Table 2. Despite their differences, all assignments attribute the bands at 1285 and 1325 cm^{-1} generally to trans conformations of the C−O and

dx.doi.org/10.1021/ma201711r |*Macromolecules* 2011, 44, 9710–9722

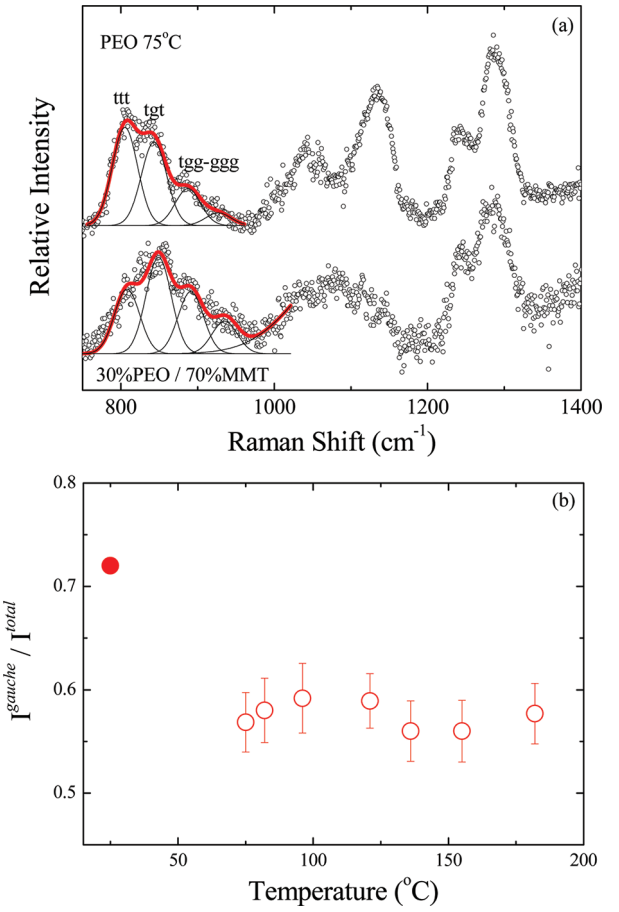

Figure 9. (a) Raman spectra of pure PEO at 75 °C and a 30 wt % PEO/Na^+-MMT nanocomposite at ambient temperature and their fitting with four Gaussians in the spectral region of CH_2 rocking vibrations. (b) Ratio of integrated intensity of the bands that correspond to gauche conformation to the total intergrated intensity in the spectral region of CH_2 rocking vibration. PEO (open circles); 30 wt % PEO/Na^+-MMT (filled circles).

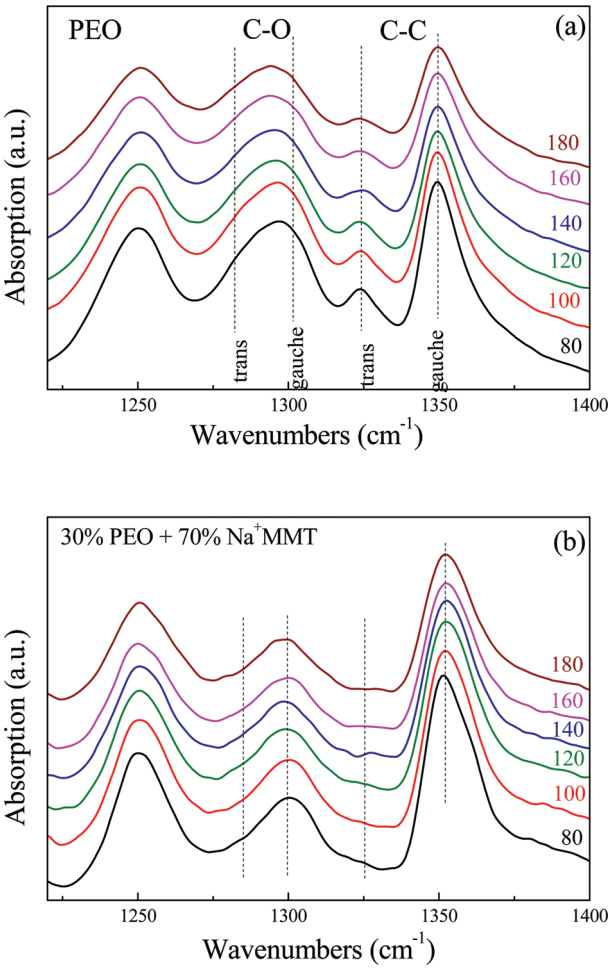

Figure 10. ATR-FTIR spectra of (a) pure PEO and (b) a 30 wt % PEO/Na^+-MMT hybrid at various temperatures above the melting transition.

C−C bonds, respectively, while the bands at 1300 and 1350 cm^{-1} are assigned basically to the respective gauche conformations. Additionally to these bands, the ones at 1460 and 1485 cm^{-1} (outside the spectral window of Figure 10) are attributed to the gauche and trans conformations of the C−C bond that are observed via the CH_2 scissoring vibration. Nevertheless, these bands will not be discussed further because there is absorption of the clay in this wavenumber range as well. The spectra of the hybrid with 30 wt % PEO show dramatic differences from those of neat PEO: the intercalated PEO chains preferably adopt gauche conformations; the bands at 1285 and 1325 cm^{-1} assigned to trans conformations of the C−O and the C−C bonds are almost vanished. Furthermore, the gauche conformations of intercalated chains appear to be more favorable compared to the respective conformations observed in neat PEO melt (the intensity ratios I^{1300}/I^{1285} and I^{1350}/I^{1325} possess much higher values for the intercalated polymer; see below). It is noted that this is a hybrid in which the majority if not all the polymer chains are confined within the inorganic galleries. This indicates that the conformations of the bulk and the confined chains are quite different even at temperatures where the pure polymer is amorphous as well.

Fittings of the infrared spectra of the pure PEO and the nanohybrid were performed utilizing a number of Gaussian functions; the ratio of the integrated intensities of the peaks attributed to trans and gauche conformations was calculated. Figure 11 shows the result of the fitting for PEO (Figure 11a) and for 30 wt % PEO + 70 wt % Na^+-MMT (Figure 11b) at 120 °C. Six to seven main bands have been utilized to successfully represent the data whereas bands to fit the ends of the curves have been used when necessary. It is noted that in all cases a baseline subtraction as well as an ATR correction have been applied before the fitting procedure. It is evident that the bands at 1325 and 1285 cm^{-1} have considerable lower intensity in the composite that in the pure polymer. On the other hand, it seems that in the case of the nanohybrid another band at ~1265 cm^{-1} is necessary to successfully fit the data. In all cases, the position of the peaks has been kept constant.

From such analysis, the ratio of the I^{gauche}/I^{total}, for the C−C and the C−O bonds, can be calculated to provide information about the effect of the inorganic walls on the conformations of the PEO chains. Figure 12a shows the ratios of the integrated intensities of $I^{1350}/(I^{1325} + I^{1350})$ and $I^{1300}/(I^{1285} + I^{1300})$, i.e., the ratio of I^{gauche}/I^{total}, for the C−C and the C−O bonds respectively, for PEO and PEO30. For pure PEO, it seems that the numbers of gauche and trans conformations are more or less similar. Nevertheless, a closer examination shows that the ratio

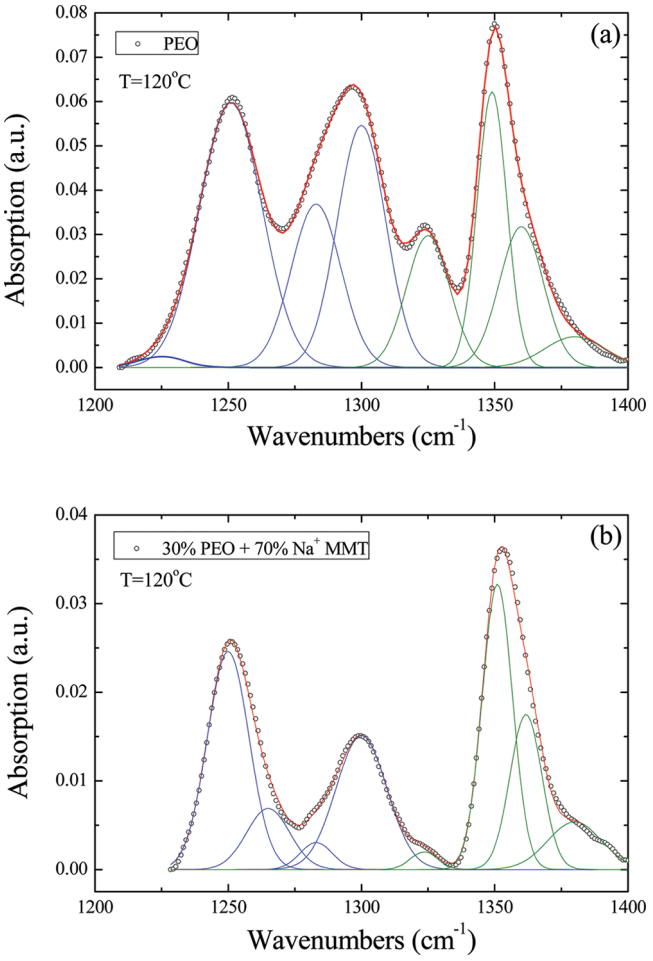

Figure 11. Fitting of ATR-FTIR spectra of (a) PEO and (b) 30 wt % PEO/Na^+-MMT hybrid at 120 °C. The lines denote the individual Gaussian peaks as well as the total fit.

$I^{1350}/(I^{1325} + I^{1350})$ is a little higher than 0.5 and increases slightly with temperature, indicating that the gauche conformation is more favorable for the C−C bond. The opposite dependence on temperature is observed for the $I^{1300}/(I^{1285} + I^{1300})$ ratio. This is in qualitative agreement with what is generally accepted for PEO according to which the energy for the gauche rotational states about the O−C and C−O bonds exceeds that of the trans state primarily because of steric interactions between adjoining methylene groups, whereas the reverse holds for the C−C bond, where a lower energy for the gauche rotational state is attributed to a favorable dispersion interactions between the oxygen atoms.[85] Moreover, there is a very good agreement between the results on the fraction of gauche conformations of the C−C bonds between the Raman and the infrared results. The situation changes severely in the case of the nanocomposite where there is a dramatic increase of the gauche conformations for both the C−C and the C−O bonds. There is even a stronger temperature dependence so that the gauche population reaches almost 100% at the highest temperature measured. Figure 12b shows the ratio of the gauche to trans population as a function of temperature, and Figure 12c shows the same data in an Arrhenius representation in order to derive the energy difference between the gauche and trans states. Previous studies of poly(ethylene oxide) suggest different values for going from the gauche to the

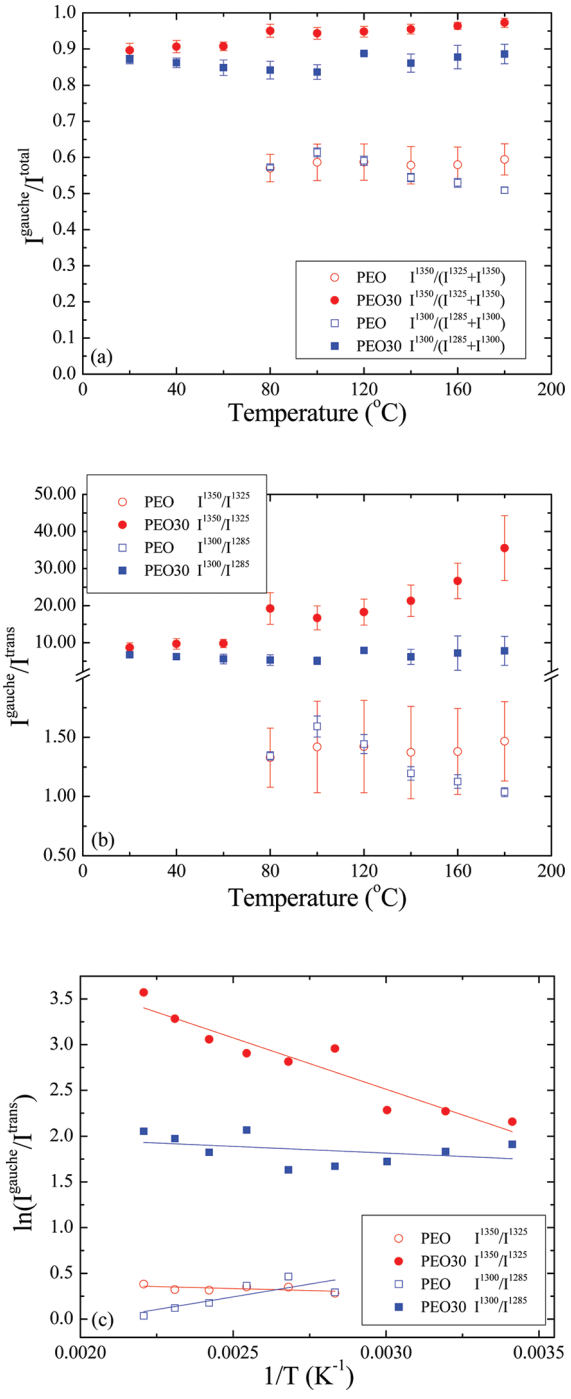

Figure 12. (a) Temperature dependence of the intensity ratios $I^{1350}/(I^{1325} + I^{1350})$, circles, and $I^{1300}/(I^{1285} + I^{1300})$, squares, signifying the I^{gauche}/I^{total} ratio for pure PEO (open symbols) and for a 30 wt % PEO/Na^+-MMT hybrid (filled symbols). (b) Temperature dependence of the intensity ratios I^{1350}/I^{1325}, circles, and I^{1300}/I^{1285}, signifying the I^{gauche}/I^{trans} ratio for pure PEO (open symbols) and for a 30 wt % PEO/Na^+-MMT hybrid (filled symbols). (c) Arrhenius representation of the data of (b) for the ratios I^{1350}/I^{1325} (circles) and I^{1300}/I^{1285} (squares) for pure PEO (open symbols) and a 30 wt % PEO/Na^+-MMT hybrid (filled symbols).

trans state for both the C−C and the C−O bonds.[85,86] In our case, it comes out that for the C−C bond the energy of the gauche state is 0.2−0.3 kcal/mol lower than the respective of the trans state; this result is in good agreement with the earlier

dx.doi.org/10.1021/ma201711r |*Macromolecules* 2011, 44, 9710–9722

studies. Moreover, this is a very low energy difference that justifies the similar number in the population of the two conformations. Nevertheless, a dramatic increase of this energy difference and thus a drastic change in the conformation of the chains are observed in the case of the nanohybrid when the polymer is confined or adsorbed on the inorganic surfaces. This is, clear from the enhanced temperature dependence of the ratio I^{gauche}/I^{trans} that leads to gauche states with 2−3 kcal/mol lower energy than the respective trans. This large energy difference is in accord with the finding that almost all C−C bonds are in the gauche conformation. It is noted that the temperature dependence was examined for the nanohybrid for the whole temperature range and not as for the pure polymer at temperatures above the T_m of PEO since it is amorphous in all cases. The energy difference for the pair of peaks that corresponds to the C−O bond indicates that the gauche state is 1−2 kcal/mol lower than the respective trans as well. Thus, our findings suggest that the favorable conformation for both the C−C and C−O bonds of the intercalated chains is the gauche one.

The findings are in agreement with previous molecular dynamics and Monte Carlo simulations,[24,55−57] which provided translational and orientational order parameters for both confined (Li^+-MMT) and neat PEO melts for various temperatures indicating that, despite the parallelism of the PEO chains to the solid walls of the inorganic component, the confined chains are "more disordered" than any of the bulk systems. Raman and IR spectroscopy indicate that this fact is a consequence of the statistically favored gauche conformations imposed by the inorganic montmorillonite layers and possibly by the cations within the galleries. Moreover, the data are in close agreement with a proposal put forward by Harris et al.,[87] who, in order to explain their findings of an increased number of C−C gauche conformations and still having the chain remained mostly planar, proposed that the chain conformations had to be alternating $gauche^+$ and $gauche^-$ and that the C−O should possess increased gauche population as well.

IV. CONCLUSIONS

X-ray diffraction, differential scanning calorimetry, and Raman and infrared spectroscopies have been utilized for the investigation of the structure of poly(ethylene oxide) chains in polymer/layered silicate nanocomposites. Intercalated nanohybrid materials with single (only for low PEO content) and double layers of polymer chains confined within the galleries are obtained when PEO is mixed with hydrophilic monmorillonite. The intercalated polymer chains as well as chains that are in close proximity to the outer surfaces of the inorganic particles remain purely amorphous; crystallinity is observed only for hybrids with high polymer content and shows an abrupt drop to zero at a certain composition. The conformation of the confined or adsorbed polymer chains, as probed by Raman and infrared spectroscopies, is found more disordered that the PEO melt even at higher temperatures. This is evident by the dramatic increase of the gauche conformations of the C−C bond along the chain backbone.

This study points at an issue that is frequently overlooked when polymer nanocomposites are investigated. Especially for the case of polymer/layered silicate composites most of the investigations focus on the modification of the structure of the inorganic particles (immiscible, intercalated, exfoliated systems) whereas not much attention has been paid to the effects of the inorganic nano- or microparticles on the conformation, structure, and even dynamics of the polymer. The present investigation shows the great influence the inorganic additives can have on the conformation and structure of the polymer: they greatly perturb the polymer crystallinity whereas they modify the chain conformations even in the noncrystallized amorphous state. The study of polymer crystallization and of the crystallization kinetics in the presence of clay particles is underway utilizing isothermal DSC as well as small-angle X-ray scattering and polarized optical microscopy measurements; it will be reported in subsequent publications. The effect of the inorganic particles on polymer dynamics has been a subject of considerable research as well.[23−31]

AUTHOR INFORMATION

Corresponding Author

*Ph + 30-2810-391255, Fax +30-2810-391305, e-mail kiki@iesl.forth.gr.

ACKNOWLEDGMENT

Part of this research was sponsored by the Greek General Secretariat for Research and Technology (Programmes ΠΕΝΕΔ 03ΕΔ581, ΠΑΒΕΤ 05PAB96 and ΣΥΝΕΡΓ ΑΣΙΑ 09ΣΥΝ-42-580), by the European Union (Programmes STREP NMP3-CT-2005-506621), and by NATO Scientific Affairs Division (Science for Peace Programme).

REFERENCES

(1) (a) Kumar, S. K.; Krishnamoorti, R. *Annu. Rev. Chem. Biol. Eng.* **2010**, *1*, 37–58. (b) Muniruzzaman, M.; Winey, K. I. *Macromolecules* **2006**, *39*, 5194–5205. (c) Bockstaller, M. R.; Mickiewicz, R. A.; Thomas, E. L. *Adv. Mater.* **2005**, *17*, 1331–1349. (d) Sharp, K. G. *Adv. Mater.* **1998**, *10*, 1243–1248.

(2) Granick, S.; Kumar, S. K.; Amis, E. J.; Antonietti, M.; Balazs, A. C.; Chakraborty, A. K.; Grest, G. S.; Hawker, C.; Janmey, P.; Kramer, E. J.; Nuzzo, R.; Russell, T. P.; Safinya, C. R. *J. Polym. Sci., Part B: Polym. Phys.* **2003**, *41*, 2755–2793.

(3) Giannelis, E. P. *Adv. Mater.* **1996**, *8*, 29–35.

(4) Le Baron, P. C.; Wang, Z.; Pinnavaia, T. J. *Appl. Clay Sci.* **1999**, *15*, 11–29.

(5) Giannelis, E. P.; Krishnamoorti, R.; Manias, E. *Adv. Polym. Sci.* **1999**, *138*, 107–147.

(6) Alexandre, M.; Dubois, P. *Mater. Sci. Eng.* **2000**, *28*, 1–63.

(7) Schmidt, D.; Shah, D.; Giannelis, E. P. *Curr. Opin. Solid State Mater. Sci.* **2002**, *6*, 205–212.

(8) Sinha Ray, S.; Okamoto, M. *Prog. Polym. Sci.* **2003**, *28*, 1539–1641.

(9) Fischer, J. *Mater. Sci. Eng., C* **2003**, *23*, 763–772.

(10) Usuki, A.; Hasegawa, N.; Kato, M. *Adv. Polym. Sci.* **2005**, *179*, 135–195.

(11) Okada, A.; Usuki, A. *Macromol. Mater. Eng.* **2006**, *291*, 1449–1476.

(12) Khrishnamoorti, R.; Vaia, R. A. *J. Polym. Sci., Part B: Polym. Phys.* **2007**, *45*, 3252–3256.

(13) Vaia, R. A.; Vasudevan, S.; Krawiec, W.; Scanlon, L. G.; Giannelis, E. P. *Adv. Mater.* **1995**, *7*, 154–156.

(14) Vaia, R. A.; Jandt, K. D.; Kramer, E. J.; Giannelis, E. P. *Macromolecules* **1995**, *28*, 8080–8085.

(15) Manias, E.; Chen, H.; Krishnamoorti, R.; Genzer, J.; Kramer, E. J.; Giannelis, E. P. *Macromolecules* **2000**, *33*, 7955–7966.

(16) Jang, B. N.; Wilkie, C. A. *Polymer* **2005**, *46*, 2933–2942.

(17) Kawasumi, M.; Hasegawa, N.; Kato, M.; Usuki, A.; Okada, A. *Macromolecules* **1997**, *30*, 6333–6338.

(18) Reichert, P.; Nitz, H.; Klinke, S.; Brandsch, R.; Thomann, R.; Mülhaupt, R. *Macromol. Mater. Eng.* **2000**, *275*, 8–17.
(19) Kim, D. H.; Fasulo, P. D.; Rodgers, W. R.; Paul, D. R. *Polymer* **2007**, *48*, 5308–5323.
(20) Hotta, S.; Paul, D. R. *Polymer* **2004**, *45*, 7639–7654.
(21) Masenelli-Varlot, K.; Vigier, G.; Vermogen, A.; Gauthier, C.; Cavaillé, J. Y. *J. Polym. Sci., Part B: Polym. Phys.* **2007**, *45*, 1243–1251.
(22) (a) Wong, S.; Vasudevan, S.; Vaia, R. A.; Giannelis, E. P.; Zax, D. B. *J. Am. Chem. Soc.* **1995**, *I17*, 7568–7569. (b) Wong, S.; Vaia, R. A.; Giannelis, E. P.; Zax, D. B. *Solid State Ionics* **1996**, *86*, 547–557.
(23) (a) Anastasiadis, S. H.; Karatasos, K.; Vlachos, G.; Manias, E.; Giannelis, E. P. *Phys. Rev. Lett.* **2000**, *84*, 915–918. (b) Anastasiadis, S. H. *J. Phys. IV* **2000**, *10*, 255–258.
(24) Kuppa, V.; Manias, E. *J. Chem. Phys.* **2003**, *118*, 3421–3429.
(25) Frick, B.; Alba-Simionesco, C.; Dosseh, G.; Le Quellec, C.; Moreno, A. J.; Colmenero, J.; Schönhals, A.; Zorn, R.; Chrissopoulou, K.; Anastasiadis, S. H.; Dalnoki-Veress, K. *J. Non-Cryst. Solids* **2005**, *351*, 2657–2667.
(26) Mijovic, J.; Lee, H. K.; Kenny, J.; Mays, J. *Macromolecules* **2006**, *39*, 2172–2182.
(27) Elmahdy, M. M.; Chrissopoulou, K.; Afratis, A.; Floudas, G.; Anastasiadis, S. H. *Macromolecules* **2006**, *39*, 5170–5173.
(28) Page, K. A.; Adachi, K. *Polymer* **2006**, *47*, 6406–6413.
(29) (a) Chrissopoulou, K.; Anastasiadis, S. H.; Giannelis, E. P.; Frick, B. *J. Chem. Phys.* **2007**, *127*, 144910−1–13. (b) Anastasiadis, S. H.; Chrissopoulou, K.; Frick, B. *Mater. Sci. Eng., B* **2008**, *152*, 33–39.
(30) Fotiadou, S.; Chrissopoulou, K.; Frick, B.; Anastasiadis, S. H. *J. Polym. Sci., Part B: Polym. Phys.* **2010**, *48*, 1658–1667.
(31) Vo, L. T.; Anastasiadis, S. H.; Giannelis, E. P. *Macromolecules* **2011**, *44*, 6162–6171.
(32) Vaia, R. A.; Sauer, B. B.; Tse, O. K.; Giannelis, E. P. *J. Polym. Sci., Part B: Polym. Phys.* **1997**, *35*, 59–67.
(33) Shen, Z.; Simon, G. P.; Cheng, Y. *Eur. Polym. J.* **2003**, *39*, 1917–1924.
(34) Chrissopoulou, K.; Afratis, A.; Anastasiadis, S. H.; Elmahdy, M. M.; Floudas, G.; Frick, B. *Eur. Phys. J.* **2007**, *141*, 267–271.
(35) Vaia, R. A.; Teukolsky, R. K.; Giannelis, E. P. *Chem. Mater.* **1994**, *6*, 1017–1022.
(36) Nam, P. H.; Maiti, P.; Okamoto, M.; Kotaka, T.; Hasegawa, N.; Usuki, A. *Polymer* **2001**, *42*, 9633–9640.
(37) Chrissopoulou, K.; Altintzi, I.; Anastasiadis, S. H.; Giannelis, E. P.; Pitsikalis, M.; Hadjichristidis, N.; Theophilou, N. *Polymer* **2005**, *46*, 12440–12451.
(38) Chrissopoulou, K.; Altintzi, I.; Andrianaki, I.; Shemesh, R.; Retsos, H.; Giannelis, E. P.; Anastasiadis, S. H. *J. Polym. Sci., Part B: Polym. Phys.* **2008**, *46*, 2683–2695.
(39) Chrissopoulou, K.; Anastasiadis, S. H. *Eur. Polym. J.* **2011**, *47*, 600–613.
(40) Manias, E. *Nature Mater.* **2007**, *6*, 9–11.
(41) Ratna, D.; Divekar, S.; Samui, A. B.; Chakraborti, B. C.; Banthia, A. K. *Polymer* **2006**, *47*, 4068–4074.
(42) Gilman, G. W. *Appl. Clay Sci.* **1999**, *15*, 31–49.
(43) Gorrasi, G.; Tortora, M.; Vittoria, V.; Pollet, E.; Lepoittevin, B.; Alexander, M.; Dubois, P. *Polymer* **2003**, *44*, 2271–2279.
(44) Shen, Z.; Simon, G. P.; Cheng, Y.-B. *Polymer* **2002**, *43*, 4251–4260.
(45) Manias, E.; Touny, A.; Wu, L.; Strawhecker, K.; Lu, B.; Chung, T. C. *Chem. Mater.* **2001**, *13*, 3516–3523.
(46) Croce, F.; Appetecchi, G. B.; Persi, L.; Scrosati, B. *Nature* **1998**, *394*, 456–459.
(47) Ruiz-Hitzky, E. *Adv. Mater.* **1993**, *5*, 334–340.
(48) Zhang, J.; Han, H.; Wu, S.; Xu, S.; Yang, Y.; Zhou, C.; Zhao, X. *Solid State Ionics* **2007**, *178*, 1595–1601.
(49) Zhang, H. C.; Zhao, Y.; Wang, J.; Zheng, H. *J. Phys. Chem. C* **2007**, *111*, 5382–5388.
(50) Kelarakis, A.; Giannelis, E. P. *Polymer* **2011**, *52*, 2221–2227.
(51) Strawhecker, K. E.; Manias, E. *Macromolecules* **2001**, *34*, 8475–8482.
(52) Strawhecker, K. E.; Manias, E. *Chem. Mater.* **2003**, *15*, 844–849.
(53) Aranda, P.; Ruiz-Hitzky, E. *Chem. Mater.* **1992**, *4*, 1395–1403.
(54) Wu, J.; Lerner, M. M. *Chem. Mater.* **1993**, *5*, 835–838.
(55) Hackett, E.; Manias, E.; Giannelis, E. P. *Chem. Mater.* **2000**, *12*, 2161–2167.
(56) Kuppa, V.; Menakanit, S.; Krishnamoorti, R.; Manias, E. *J. Polym. Sci., Part B: Polym. Phys.* **2003**, *41*, 3285–3298.
(57) Kuppa, V.; Manias, E. *J. Polym. Sci., Part B: Polym. Phys.* **2005**, *43*, 3460–3477.
(58) Tadokoro, H.; Chatani, Y.; Yoshihara, T.; Tahara, S.; Murahashi, S. *Macromol. Chem. Phys.* **1964**, *73*, 109–127.
(59) Takahashi, Y.; Sumita, I.; Tadokoro, H. *J. Polym. Sci., Polym. Phys.* **1973**, *11*, 2113–2122.
(60) Bortel, E.; Hodorowicz, S.; Lamot, R. *Macromol. Chem. Phys.* **1979**, *180*, 2491–2498.
(61) Saujanya, C.; Radhakrishnan, S. *J. Appl. Polym. Sci.* **1997**, *65*, 1127–1137.
(62) (a) Homminga, D.; Goderis, B.; Dolbnya, I.; Reynaers, H.; Groeninckx, G. *Polymer* **2005**, *46*, 11359–11365. (b) Hindeleh, A. M.; Jonhson, D. J. *Polymer* **1978**, *19*, 27–32.
(63) It is noted that this calculation explicitly assumes that the contribution of the clay in this range of scattering angles can be considered negligibly small.[62a]
(64) Chaiko[65] shows an XRD pattern (Figure 7) for a PEO-1450/H^+-saponite containing 50 wt% PEO, where "the 4.63 and 3.82 Å reflections from the PEO crystal are absent", as well as a DSC trace on the same specimen, where a melting endotherm is seen. Most probably, for that particular polymer/clay system this composition falls in the regime that was drawn as a grey region in Figure 3. Moreover, Stefanescu et al.[66] for a PEO-1 000 000/Na^+-MMT nanocomposite containing 40 wt % PEO show similarly DSC traces indicating crystallinity and XRD data where the peaks for crystalline PEO were absent.
(65) Chaiko, D. J. *Chem. Mater.* **2003**, *15*, 1105–1110.
(66) Stefanescu, E. A.; Dundigalla, A.; Ferreiro, V.; Loizou, E.; Porcar, L.; Negulescu, I.; Garno, J.; Schmidt, G. *Phys. Chem. Chem. Phys.* **2006**, *8*, 1739–1746.
(67) Kuppa et al.[56] presents a figure (Figure 14) that shows enthalpy of melting data measured in PEO/Na^+-MMT nanocomposites. In that case, one does not see the "jump" in crystallinity as in our Figure 3. The apparent "jump" observed between 40 and 20 wt % PEO is probably because in the 20 wt % all polymer is inside the galleries. However, since no information is given in that paper on the characteristics of the polymer, one cannot speculate whether differences in the polymer characteristics (and/or preparation conditions) could explain the difference from our observations.
(68) The use of Scherrer equation is only approximate, and someone should have in mind that many parameters like the coherence and/or a possible interstratification of the structure could affect the width of the peak and, thus, the estimated size.
(69) Klonos, P.; Panagopoulou, A.; Bokobza, L.; Kyritsis, A.; Peoglos, V.; Pissis, P. *Polymer* **2010**, *51*, 5490–5499.
(70) The kinetics of crystallization was independently investigated[71] for nanohybrids with PEO content higher than 90 wt %. The results showed that the crystallization times, for temperatures 10−20 deg lower than the melting temperature, are always less than 3000 s, with the longer times corresponding to the higher crystallization temperatures; the results on the crystallization kinetics will be reported in a subsequent publication. Thus, the kinetics of crystallization, which in principle is influenced by the polymer molecular weight, the crystallization temperature, the cooling rate, etc., does not interfere with the present investigation.
(71) Papananou, H.; Chrissopoulou, K.; Anastasiadis, S. H., manuscript in preparation.
(72) Mirabella, F. M.; Bafna, A. *J. Polym. Sci., Part B: Polym. Phys.* **2002**, *40*, 1637–1643.
(73) Hisokaka, M. Y.; Pulcinelli, S. H.; Santilli, C. V.; Dahmouche, K.; Craievich, A. F. *J. Non-Cryst. Solids* **2006**, *352*, 3705–3710.
(74) Zaky, M. T.; Mohamed, N. H. *Thermochim. Acta* **2010**, *499*, 79–84.

(75) Lima, M. F. S.; Vasconcellos, M. A. Z.; Samios, D. *J. Polym. Sci., Part B: Polym. Phys.* **2002**, *40*, 896–903.
(76) (a) Strobl, G. R.; Hagedorn, W. *J. Polym. Sci., Part B: Polym. Phys.* **1978**, *16*, 1181–1193. (b) Mutter, R.; Stille, W.; Strobl, G. *J. Polym. Sci., Part B: Polym. Phys.* **1993**, *31*, 99–105.
(77) Nielsen, A. S.; Batchelder, D. N.; Pyrz, R. *Polymer* **2002**, *43*, 2671–2676.
(78) Flory, P. J. *Statistical Mechanics of Chain Molecules*; Interscience Publishers: New York, 1969.
(79) Yang, X.; Su, Z.; Wu, D.; Hsu, S. L.; Stidham, H. D. *Macromolecules* **1997**, *30*, 3796–3802.
(80) It is mentioned that the Raman signal weakens as PEO concentration is further reduced, and at ~20% the quality of the spectra offers no possibility even for qualitative results.
(81) Koening, J. L.; Angood, A. C. *J. Polym. Sci., Part A-2* **1970**, *8*, 1787–1796.
(82) Maxfield, J.; Shepherd, I. W. *Polymer* **1975**, *16*, 505–509.
(83) (a) Matsuura, H.; Miyazawa, T. *J. Polym. Sci., Part A-2* **1969**, *7*, 1735–1744. (b) Matsuura, H.; Fukuhara, K. *J. Polym. Sci., Part B: Polym. Phys.* **1986**, *24*, 1383–1400. (c) Begum, R.; Matsuura, H. *J. Chem. Soc., Faraday Trans.* **1997**, *93*, 3839–3848.
(84) The percentage of the *tgt* triads in the nanocomposite can be estimated from Figure 9a as 36% at 25 °C, which is not so different from the value of 47−50% reported by Kuppa et al.[57] Note that comparison with the data for the PEO melt cannot be made since the simulations were performed in the presence of Li^+, which, in principle, can influence the conformation.
(85) (a) Mark, J. E.; Flory, P. J. *J. Am. Chem. Soc.* **1965**, *87*, 1415–1423. (b) Mark, J. E.; Flory, P. J. *J. Am. Chem. Soc.* **1966**, *88*, 3702–3707.
(86) Abe, A.; Mark, J. E. *J. Am. Chem. Soc.* **1976**, *98*, 6470–6476 and references therein.
(87) Harris, D. J.; Bonagamba, T. J.; Schmidt-Rohr, K. *Macromolecules* **1999**, *32*, 6718.